

# Detection of $c$ , $d$ , and $e$ waves in the acceleration photoplethysmogram

Mohamed Elgendi

Computing Science Department, University of Alberta, Canada

August 11, 2014

## **Abstract**

Analyzing the acceleration photoplethysmogram (APG) is becoming increasingly important for diagnosis. However, processing an APG signal is challenging, especially if the goal is to detect its small components ( $c$ ,  $d$ , and  $e$  waves). Accurate detection of  $c$ ,  $d$ , and  $e$  waves is an important first step for any clinical analysis of APG signals. In this paper, a novel algorithm that can detect  $c$ ,  $d$ , and  $e$  waves simultaneously in APG signals of healthy subjects that have low amplitude waves, contain fast rhythm heart beats, and suffer from non-stationary effects was developed. The performance of the proposed method was tested on 27 records collected during rest, resulting in 97.39% sensitivity and 99.82% positive predictivity.

## **1 Introduction**

The pulse wave analysis provides more precise information concerning blood pressure changes than systolic and diastolic pressures only[1]. It is a valuable method to assess aortic stiffness and elasticity [2, 3, 4], and to evaluate

the vascular effects of aging, hypertension, and atherosclerosis [5, 6, 7, 8]. Photoplethysmography (pulse oximeter) is the most common device used to measure pulse waves, which illuminates the skin and measures changes in light absorption. The measured signal has been referred to as photoplethysmogram (PTG/PPG) and digital volume pulse (DVP); however, the acronym PPG will be used exclusively within this study, according to the recommendations in [9]. Fingertip PPG mainly reflects the pulsatile volume changes in the finger arterioles, as shown in Figure 1.

For more accurate recognition of the inflection points and easier interpretation of the pulse wave, the second derivative of the original plethysmogram wave was introduced [10]. The acronym of the second derivative PPG is SDPPG or APG; however, the acronym APG will be used exclusively in this study, according to the recommendations in [9].

As shown in Figure 1, the waveform of the APG consists of four systolic waves ( $a$ ,  $b$ ,  $c$ , and  $d$  waves) and one diastolic wave ( $e$  wave) [11]. The height of each wave was measured from the baseline, with the values above the baseline being positive and those under it negative. The relative heights of these waves ( $b/a$ ,  $c/a$ ,  $d/a$ , and  $e/a$  ratios), particularly the  $c/a$  ratio has been related to arterial stiffness and aging [7, 12] and essential hypertension [13]. All these ratios were used in calculating the ageing index  $(b - c - d - e)/a$  [7]. Recently, the detection of  $a$  waves in APG signals has been used to calculate heart rate [14, 15, 16] and heart rate variability indexes [17, 18]. Moreover, Homma et al. [19] categorized the APG into seven types depending on the waveforms. The clinical description of these categories has been demonstrated in Figure 2.

Although the clinical significance of APG measurement has been well investigated, there is still a lack of studies focusing on the automatic detec-

tion of  $c$ ,  $d$  and  $e$  waves in APG signals. However, there was an attempt by Matsuyama [20] to determine which of the nine QRS algorithms of Friesen's ECG algorithms [21] suits the detection of  $a$  waves in APG signals. However, up to the present, there has been no attempt to detect  $c$ ,  $d$ , and  $e$  waves in APG signals; therefore, this investigation aimed to develop an algorithm to detect  $c$ ,  $d$ , and  $e$  waves in APG signals. To test the robustness of the developed algorithm, noisy PPG signals (measured after exercise) were used.

## 2 Materials and Methods

### 2.1 Ethics Statement

The PPG data were collected as a minor part of a joint project between Charles Darwin University (Darwin, Northern Territory, Australia), the Defence Science and Technology Organisation (DSTO), and the Department of Defence and was initiated by the Department of Defence [20]. The main aim of the project was to assess the effect of varying degrees of airconditioning exposure in hot environments [20]. The project has been granted human research ethic clearance from Charles Darwin University [20]. Only de-identified numerical data, representing PPG signals as vectors, are stored on the database. The database is available upon request at Charles Darwin University: <http://www.cdu.edu.au/ehse>.

### 2.2 Database Used

There are currently no standard PPG databases with annotated  $c$ ,  $d$  and  $e$  waves available to evaluate the developed algorithms. One annotated PPG database is available at Charles Darwin University. The data were collected during rest (before exercise) and after one hour of exercise (walking) on a

treadmill in the climate control chamber at Northern Territory Institution of Sport (Darwin, Australia). The speed of treadmill was set to 5 km/h with a one percent increment corresponding to the effort required to walk with 8 kg of webbing. The exercise was considered to be of moderate intensity, and the background of the entire project can be found in [20].

PPGs of 27 healthy volunteers (males) with a mean  $\pm$  SD age of  $27 \pm 6.9$  were measured using a photoplethysmography device (Salus APG, Japan), with the sensor located at the cuticle of the second digit of the left hand, in which all subjects were included. Measurements were taken while the subject was at rest on a chair. PPG data were collected at a sampling rate of 200 Hz and the duration of each recording was 20 seconds. For signal conditioning and wave detection, MATLAB 2010b (The MathWorks, Inc., Natick, MA, USA) was used.

### **2.2.1 Training Set**

The PPG signals collected after one hour of exercise were used for training as they includes different shapes of PPG waveforms and noise. Moreover, they contained fast rhythm PPG signals, with a total of 885 heart beats, which had an impact on the detection accuracy.

### **2.2.2 Test Set**

PPG signals measured during rest (before exercise), with a total of 584 heart beats, were used for testing as they contain different morphologies of the *c*, *d*, and *e* waves. They also include different types of noises, such as power-line interferences (50 Hz and its harmonics, see Fig. 3 (a)), low amplitude signals (see Fig. 3(b)), as well as low-frequency baseline fluctuations (see Fig. 3(c, d, e)) and irregular heart beats (see Fig. 3(e)).

## 2.3 Methodology

In this study, a novel algorithm, adapted from the framework proposed by Elgendi to detect systolic waves in PPG signals [22] and QRS complexes in ECG signals [23], will be evaluated. The same approach will be used here to detect the *c*, *d*, and *e* waves. The method consists of three main stages: pre-processing (bandpass filtering, second derivative, and cancellation of *a* and *b* waves), feature extraction (generating blocks of interest using two moving averages), and classification (thresholding). The structure of the algorithm is given in Figure 4.

### 2.3.1 Bandpass Filter

A zero-phase second-order Butterworth filter, with a bandpass of 0.5–7 Hz based on a brute force search that will be discussed later in the parameter optimization section, was implemented to remove unwanted noise and possible movement artefacts (cf. Figure 3). The output of the zero-phase Butterworth filter applied to the PPG signal produced a filtered signal  $S[n]$ . The code line of this step is line 2 in the pseudocode of the *c*, *d*, and *e* waves detection algorithm (Algorithm I).

### 2.3.2 Second Derivative

To obtain the APG signals, the second derivative was applied to the filtered PPG in order to analyse the APG signals. Equations 1 and 2 represent a non-causal filter; the three-point center derivative was created with a delay of only two samples.

$$S'[n] = \left. \frac{dS}{dt} \right|_{t=nT} = \frac{1}{2T}(S[n+1] - S[n-1]), \quad (1)$$

$$\text{APG}[n] = \left. \frac{dS'}{dt} \right|_{t=nT} = \frac{1}{2T}(S'[n+1] - S'[n-1]), \quad (2)$$

where  $T$  is the sampling interval and equals the reciprocal of the sampling frequency, and  $n$  is the data sample. Figure 5(a) shows the second derivative of the filtered PPG signal measured. The code line of this step is line 3 in the pseudocode of the proposed detector (Algorithm I).

### 2.3.3 Removal of $a$ and $b$ waves

At this stage, the  $cde$  segment of the APG needs to be emphasized to distinguish it clearly for detection. This can be done by removing the  $a$  and  $b$  waves from the APG signal, as follows:

$$\text{APG}(a_{\text{waves}}(i) - \text{cutoff} : a_{\text{waves}}(i) + \text{cutoff}) = 0, \quad (3)$$

where  $i$  is the number of  $a$  waves (the peaks of  $a$  waves), while the **cutoff** represents the area before or after the peak of the  $a$  wave. The exact value for a **cutoff** of 30 ms (6 samples for a sampling frequency of 200 Hz) is determined after a brute force search, which will be discussed later in the parameter optimization section. The code line of this step is line 4 in the pseudocode of the proposed detector (Algorithm I).

### 2.3.4 Generating Blocks of Interest

Blocks of interest are generated using two moving averages that demarcate the  $c$  and  $e$  waves and  $cde$  segment areas. The particular method used to generate blocks of interest has been mathematically shown to detect systolic waves [22] and QRS complexes [23].

In this procedure, the first moving average ( $\text{MA}_{\text{peak}}$ ) is used to emphasise the  $c$  and  $e$  waves area, as the dotted signal shows in Figure 5(b), and is

given by

$$\text{MA}_{\text{peak}}[n] = \frac{1}{W_1} (y[n - (W_1 - 1)/2] + \dots + y[n] + \dots + y[n + (W_1 - 1)/2]), \quad (4)$$

where  $W_1$  represents the window size of  $c$  or  $e$  wave duration. The resulting value is rounded to the nearest odd integer. The exact value for  $W_1$  of 5 ms is determined after a brute force search, which will be discussed later in the parameter optimization section.

The second moving average ( $\text{MA}_{\text{cde}}$ ) is used to emphasize the beat area to be used as a threshold for the first moving average, shown as a dashed signal in Figure 5(b), and is given by

$$\text{MA}_{\text{cde}}[n] = \frac{1}{W_2} (y[n - (W_2 - 1)/2] + \dots + y[n] + \dots + y[n + (W_2 - 1)/2]), \quad (5)$$

where  $W_2$  represents a window size of approximately the duration of the  $cde$  segment that contains the  $c$ ,  $d$ , and  $e$  waves. Its value is rounded to the nearest odd integer. The exact value for  $W_2$  of 15 ms is determined after a brute force search, which will be discussed later in the parameter optimization section. Applying the  $\text{MA}_{\text{cde}}$  as a threshold for the  $\text{MA}_{\text{peak}}$  generates blocks of interest. The code lines of this step are lines 5–14 in the pseudocode of the proposed detector (Algorithm I).

### 2.3.5 Thresholding

In this stage, the blocks of interest were generated, some of which will contain the  $c$  and  $e$  waves and some of which will primarily contain noise. Therefore, the next step is to reject blocks that result from noise. Rejection is based on

the peak width and its relative distance to the  $a$  peak. Regarding the peak width (the duration of  $c$ ,  $d$ , or  $e$  wave), it was determined in the previous step, during the calculation of  $MA_{\text{peak}}$ ; thus, the width threshold is

$$\text{THR}_1 = W_1. \quad (6)$$

In order to determine whether the detected blocks contain  $c$  or  $e$  waves, the number of blocks in each consecutive  $aa$  interval is first counted. Two thresholds (or search areas) are then applied based on the relative distance between the detected blocks and its current  $a$  wave, as shown in Figure 6. The minimum search distance for  $c$  wave is defined as

$$AC_{\min} = (aa/f_s) * ac_{\min}, \quad (7)$$

while the maximum search distance for  $e$  wave is defined as referred to as

$$AE_{\max} = (aa/f_s) * ae_{\max}, \quad (8)$$

where  $f_s$  refers to the sampling frequency, and the  $aa$  is the interval between the current  $a$  wave and the next  $a$  wave. The value of  $ac_{\min}$  and  $ae_{\max}$  is fixed; however, the value of  $AC_{\min}$  and  $AE_{\max}$  is the adapted to the heart rate ( $aa$  interval). The code lines of this step are lines 17–20 in the pseudocode of the proposed algorithm (Algorithm I). The exact values of  $ac_{\min}$  and  $ae_{\max}$  are determined after a brute force search, which will be discussed later in the parameter optimization section.

By applying the width threshold ( $W_1$ ) along with the two search thresholds ( $AC_{\min}$  and  $AE_{\max}$ ), there will be two possibilities for the number of detected blocks:

1. More than one block: the first block (maximum value within the first block) is considered a  $c$  wave, while the second block (maximum value within the second block) is considered a  $e$  wave, as shown in cases 1 and 2 in Figure 5(b). Moreover, the minimum value that lies between the detected  $c$  wave and the detected  $e$  wave is considered  $d$  wave. The code lines of this step are lines 30–33 in the pseudocode of the proposed algorithm (Algorithm I).
2. One block: the  $c$ ,  $d$  and  $e$  waves are most likely merged within one block, as shown in case 3 in Figure 5(b). The  $c$ ,  $d$ , and  $e$  waves are usually merged in APG signals measured after exercise. The code lines of this step are lines 35–37 in the pseudocode of the proposed algorithm (Algorithm I).

The detected waves were compared to the annotated waves, within a search range of  $\pm 5$  ms for all waves.

### 2.3.6 Parameter Optimization

Performance of  $c$ ,  $d$ , and  $e$  waves detection algorithms is typically evaluated using two statistical measures:

$SE = TP/(TP + FN)$  and  $+P = TP/(TP + FP)$ , where  $TP$  is the number of true positives ( $c/d/e$  wave detected as  $c/d/e$  wave),  $FN$  is the number of false negatives ( $c/d/e$  wave has not been detected), and  $FP$  is the number of false positives (non- $c/d/e$  wave detected as  $c/d/e$  wave). The sensitivity  $SE$  reported the percentage of true  $c/d/e$  waves that were correctly detected by the algorithm. The positive predictivity  $+P$  reports the percentage of the detected  $c/d/e$  waves that were true  $c/d/e$  waves. Similarly, the same statistical measures were used to evaluate the  $b$  waves.

The function of the  $c$ ,  $d$ , and  $e$  waves detector (cf. pseudocode of Algorithm I) has ten inputs: the PPG signal ( $PPG_{\text{signal}}$ ), frequency band ( $F_1-F_2$ ), and event-related durations  $W_1, W_2$ , **cutoff**,  $ac_{\min}$ ,  $ae_{\max}$ ,  $a_{\text{waves}}$ ,  $b_{\text{waves}}$ , and  $f_s$ . Any change in these parameters will affect the overall performance of the proposed algorithm. These parameters are interrelated and cannot be optimized in isolation. A rigorous optimization, brute-force search based on the knowledge-base information, over all parameters, is conducted, as shown in Algorithm II. This is time consuming, as the complexity of the algorithm is  $O((Max_{F_1} - F_1) \times Max_{F_2} - F_2) \times (Max_{W_1} - W_1) \times (Max_{W_2} - W_2) \times (Max_{\text{cutoff}} - \text{cutoff}) \times (Max_{ac_{\min}} - ac_{\min}) \times (Max_{ae_{\max}} - ae_{\max}))$ , but it is required before making any claims.

The data used in this training phase were the PPG signals measured at after 1 hour of exercise. All possible combinations of parameters (26,000 iterations) have been investigated and sorted in descending order according to their overall accuracy (the average value of SE and +P), as shown in Table 3. Note, the parameters were optimized separately for each subject within the training data.

Optimization of the beat detector’s spectral window for the lower frequency resulted in a value within 0.5–1 Hz with the higher frequency within 4–10 Hz. The window size of the first moving average ( $W_1$ ) varied from 5–25 ms, whereas the window size of the second moving average ( $W_2$ ) varied from 10–15ms. The **cutoff** was tested over the range 30–70 ms, and  $ac_{\min}$  was tested over the range 0–40 ms, while the  $ae_{\max}$  was tested over the range 300–600 ms. It is clear from Table 3 that the optimal frequency range for the detection algorithm over the database was 0.5–7 Hz. Moreover, the optimal values for the moving-average window sizes and offset were  $W_1 = 5$  ms,  $W_2 = 15$  ms, **cutoff** = 30 ms,  $ac_{\min} = 10$  ms, and  $ae_{\max} = 500$  ms. The  $c$ ,

$d$ , and  $e$  detection algorithm was adjusted with these optimal parameters. The detector was then tested on PPG measured during rest without any further adjustment.

### 3 Results and Discussion

The algorithm was tested on 27 subjects with PPG signals measured at two time points: before exercise and after exercise, with a total number of 54 recordings. The main objective is to evaluate the robustness of the algorithm against the non-stationary effects, low SNR, and high heart rate exhibited after exercise. Under controlled conditions (e.g., hospital and clinic), analyzing stationary APG signals is easier [24]; as  $c$ ,  $d$ , and  $e$  waves have similar amplitudes, the statistical characteristics of the signals (i.e., mean and standard deviation) do not change appreciably with time, and a simple threshold level can effectively detect systolic peaks. Figure 7(a) represents the APG signals with stationarity effects for volunteer G3 (before exercise) with  $c$ ,  $d$ , and  $e$  peaks that are almost straight-lined. Also, Figure 7(c) represents the APG signals with stationarity effects in a fast heart rate for volunteer G2 (before exercise); however, in this case the  $c$ ,  $d$ , and  $e$  peaks are almost merged. By contrast, non-stationary APG signals makes analysis difficult since the standard deviation changes with time ( $c$ ,  $d$ , and  $e$  wave amplitudes vary with time, and simple level thresholds cannot optimally detect them). This has a negative effect on detection algorithm performance, especially PPG signals collected during rest.

PPG signals collected after exercises suffered from low and high frequencies because of the sweat and exhaustion of the volunteer; however, the bandpass filter succeeded in removing these artifacts. It is worth noting that the detection accuracy of any algorithm will increase for PPG signals

collected after exercise. This is because of the fast rhythm caused by the stress test, which decreases the time duration between two consequent heart pulses. This will cause a merge of the  $c$ ,  $d$ , and  $e$  peaks, and therefore, the detection of the merged waves will be easier (cf. Figure 7(c)). It is important to mention that the merging of  $c$ ,  $d$ , and  $e$  peaks in the case of fast heart rhythm is not caused by filtering, as shown in Figure 8.

The results show that the proposed detector is able to detect  $c$ ,  $d$ , and  $e$  peaks correctly in non-stationary APG signals before exercise, as shown in Figures 7(a and c). The proposed algorithm succeeded in detecting  $c$ ,  $d$ , and  $e$  in APG signals with irregular heart beats (cf. Figure 7(b)) and APG signals with low amplitude (cf. Figure 7(d)). The detector scored an SE of 99.8% and +P of 99.82% in detecting  $c$  waves, an SE of 92.7% and +P of 100% in detecting  $d$  waves, and an SE of 99.64% and +P of 99.64% in detecting  $e$  waves, as shown in Table 4. However, in the case of non-stationary APG signals, the algorithm did incur a few instances of failure; see Figure 9, Figure 10, and Figure 11. The detector incurred one FP and one FN for detecting  $c$  waves, 18 FNs for detecting  $d$  waves, and two FPs and two FNs for detecting  $e$  waves. The cause of the failure to detect  $c$  waves is due to the extremely low amplitude  $c$  waves in APG signals during rest (cf. Figure 9), which also caused indirect failure to detect  $d$  waves. In other words, the  $d$  waves do not have a clear minimum value between the  $c$  and  $e$  waves. Developing a robust  $d$  waves detection algorithm needs more investigation. In such cases, applying a simple level threshold to detect  $c$ ,  $d$ , or  $e$  waves is not an effective approach. The proposed method, however, handles varying amplitudes, as shown Figure 7. In fact, it is clear that the proposed algorithm is more amplitude-independent and is able to detect the  $c$ ,  $d$ , and  $e$  waves in various voltage ranges.

The analysis of a regular heart rhythm is simple, as the systolic peaks are repeated with an equally spaced pattern. This regularity helps the time-domain threshold methodologies to detect  $c$ ,  $d$ , and  $e$  peaks successfully. The regular heart rhythm is called the normal sinus rhythm in APG signals [25], which means the rhythm is constant and the occurrence of the next beat is predictable. The proposed algorithm easily detects systolic peaks correctly in PPG signals with a regular heart rhythm, as shown in Figure 7(a). The sensation of an irregular heart rhythm is usually related to either premature beats or atrial fibrillation. The proposed algorithm is able to detect  $c$ ,  $d$ , and  $e$  peaks with premature beats, as shown in Figure 7(b).

## 4 Limitations of the Study and Future Work

The proposed method only tested on healthy subjects. The physiology of the photoplethysmogram significantly changes according to the health status. As such, the robustness of the proposed method needs to be verified by a study in unhealthy subjects. One of the next steps regarding the results of this study is to examine the  $c/a$ ,  $d/a$ , and  $e/a$  ratios (based on the accurately detected  $c$ ,  $d$ , and  $e$  waves) using APG signals in diagnosis and monitoring abnormality such as arrhythmia, hypertension, diabetes and hyperlipidemia. It is important to note that the PPG signals were collected from 27 healthy male subjects, a larger sample size and a more diverse data set are needed in order to generalize the findings of this study. Moreover, sampling the PPG signals at a higher rate (above 200 Hz) is required to capture the  $c$ ,  $d$ , and  $e$  waves more clearly. The evaluation of  $c$  and  $d$  wave detection was challenging in this study because the database did not contain all possible morphologies found in APG signals, especially for unhealthy subjects. To our knowledge, there is no available APG database with annotated  $c$ ,  $d$ , and

*e* waves that would allow a more thorough assessment and comparison of the tested algorithm.

## 5 Conclusion

Currently, a full understanding of the diagnostic value of the different features of the APG signal is still lacking, and more research is needed. Moreover, the detection algorithm of *c*, *d*, and *e* waves in APG signals has not been previously addressed in the literature. However, a robust algorithm has been proposed to detect *c*, *d*, and *e* waves simultaneously in APG signals with high-frequency noise, low amplitude, non-stationary effects, and irregular heart beats. The detection errors arose mainly from low amplitude *c* and *e* peaks relative to the *d* peak. The algorithm was evaluated using 27 records, containing 584 heart beats, with an overall sensitivity of 97.39% and an overall positive predictivity of 99.82%.

## 6 Acknowledgments

I would like to gratefully acknowledge the Australian government and Charles Darwin University, as their generous scholarships facilitated this research. I appreciate the support of Prof. Friso De Boer, who provided access to the PPG database and valuable comments, and I acknowledge Dr. Gari Clifford for the helpful discussions.

## 7 References

### References

- [1] Takazawa K, Tanaka N, Takeda K, Kurosu F, Ibukiyama C (1995) Underestimation of vasodilator effects of nitroglycerin by upper limb blood pressure. *Hypertension* 26: 520–523.
- [2] Chrife R, Pigott V, Spodick D (1971) Measurement of the left ventricular ejection time by digital plethysmography. *American Heart Journal* 82: 222–227.
- [3] Kelly R, Hayward C, Avolio A, O’Rourke M (1989) Noninvasive determination of age-related changes in the human arterial pulse. *Circulation* 80: 1652–1659.
- [4] O’Rourke M, Avolio A, Kelly R (1992) *The Arterial Pulse*. Baltimore: Lea & Febiger.
- [5] Darne B, Girerd X, Safar M, Cambien F, Guize L (1989) Pulsatile versus steady component of blood pressure: a cross-sectional analysis and a prospective analysis on cardiovascular mortality. *Hypertension* 13: 392–400.
- [6] Barenbrock M, Spieker C, Kerber S, Vielhauer C, Hoeks A, et al. (1995) Different effects of hypertension, atherosclerosis and hyperlipidemia on arterial distensibility. *Hypertension* 13: 1712–1717.
- [7] Takazawa K, Tanaka N, Fujita M, Matsuoka O, Saiki T, et al. (1998) Assessment of vasoactive agents and vascular aging by the second derivative of photoplethysmogram waveform. *Hypertension* 32: 365–370.

- [8] Bortolotto A, Jacques B, Takeshi K, Kenji T, Michel S (2000) Assessment of vascular aging and atherosclerosis in hypertensive subjects: second derivative of photoplethysmogram versus pulse wave velocity. *American Journal of Hypertension* 13: 165–171.
- [9] Elgendi M (2012) Standard terminologies for photoplethysmogram signals. *Current Cardiology Reviews* 8: 215–219.
- [10] Seki H (1977) Classification of wave contour by first and second derivative of plethysmogram (in japanese). *Pulse Wave* 7: 42-50.
- [11] Takazawa K, Fujita M, Kiyoshi Y, Sakai T, Kobayashi T, et al. (1993) Clinical usefulness of the second derivative of a plethysmogram (acceleration plethysmogram). *Cardiology* 23: 207–217.
- [12] Baek HJ, Kim JS, Kim YS, Lee HB, Park KS (2007) Second derivative of photoplethysmography for estimating vascular aging. In: the 6th International Special Topic Conference on Information Technology Applications in Biomedicine (ITAB 2007), Tokyo, Japan. pp. 70–72. doi:10.1109/ITAB.2007.4407346.
- [13] Šimek J, Wichterle D, Melenovsky V, Malik J, Savacina S, et al. (2005) Second derivative of the finger arterial pressure waveform: An insight into dynamics of the peripheral arterial pressure pulse. *Physiological Research* 54: 505–513.
- [14] Allen J (2007) Photoplethysmography and its application in clinical physiological measurement. *Physiological Measurement* 28: R1–R39.
- [15] Taniguchi K, Nishikawa A, Nakagoe H, Sugino T, Sekimoto M, et al. (2007) Evaluating the surgeon’s stress when using surgical assistant

- robots. In: The 16th IEEE International Symposium on Robot and Human interactive Communication (RO-MAN 2007). pp. 888–893.
- [16] Elgendi M, Jonkman M, De Boer F (2009) Measurement of  $a-a$  intervals at rest in the second derivative plethysmogram. In: the IEEE 2009 International Symposium on Bioelectronics and Bioinformatics, RMIT University, City Campus Melbourne, Australia. pp. 75–79.
- [17] Elgendi M, Jonkman M, De Boer F (2011) Heart rate variability and acceleration plethysmogram measured at rest. In: Fred A, Filipe J, Gamboa H, editors, Biomedical Engineering Systems and Technologies, Springer, Communications in Computer and Information Science. pp. 266–277.
- [18] Lin CH (2011) Assessment of bilateral photoplethysmography for lower limb peripheral vascular occlusive disease using color relation analysis classifier. *Computer Methods and Programs in Biomedicine* 103: 121–131.
- [19] Homma S, Ito S, Koto T, Ikegami H (1992) Relationship between accelerated plethysmogram, blood pressure and arterial elasticity. *The Japanese Society of Physical Fitness and Sport Medicine* 41: 98–107.
- [20] Matsuyama A (2009) ECG and APG Signal Analysis during Exercise in a Hot Environment. PhD Thesis, Charles Darwin University, Darwin, Australia.
- [21] Friesen GM, Jannett TC, Jadallah MA, Yates SL, Quint SR, et al. (1990) A comparison of the noise sensitivity of nine QRS detection algorithms. *IEEE Trans Biomedical Engineering* 37: 85–98.

- [22] Elgendi M, Norton I, Brearley M, Abbott D, Schuurmans D (2013) Systolic peak detection in acceleration photoplethysmograms measured from emergency responders in tropical conditions. PLoS ONE. doi:10.1371/journal.pone.0076585. In press.
- [23] Elgendi M (2013) Fast QRS detection with an optimized knowledge-based method: Evaluation on 11 standard ECG databases. PLoS ONE 8: e73557.
- [24] Lei WK, Dong MC, Fang WX, Hu XY (2012) An approach towards realizing the intelligent sphygmogram sampling for e-home healthcare. Computer Methods and Programs in Biomedicine 108: 1199–1205.
- [25] Braunwald E, Zipes D, Libby P, Bonow R (2004) Braunwald’s Heart Disease: A Textbook of Cardiovascular Medicine. Philadelphia: Saunders, 7th edition.
- [26] Elgendi M (2012) On the analysis of fingertip photoplethysmogram signals. Current Cardiology Reviews 8: 14–25.

## 8 Tables

Table 1: **Pseudocode for the knowledge-based  $c$ ,  $d$ , and  $e$  waves detector.** The function has ten inputs:  $PPG_{\text{signal}}$ ,  $f_s$ ,  $a_{\text{waves}}$ ,  $b_{\text{waves}}$ , frequency band ( $F_1$ – $F_2$ ),  $W_1$  (samples),  $W_2$  (samples), **cutoff** (samples),  $ac_{\text{min}}$  (samples), and  $ae_{\text{max}}$  (samples). The data used in this training phase were PPG signals measured after 1 hour of exercise.

---

**Algorithm I:** DETECTOR( $PPG_{\text{signal}}$ ,  $f_s$ ,  $a_{\text{waves}}$ ,  $b_{\text{waves}}$ ,  $F_1$ ,  $F_2$ ,  $W_1$ ,  $W_2$ , **cutoff**,  $ac_{\text{min}}$ ,  $ae_{\text{max}}$ )

---

```

1 :  $c_{\text{waves}} \leftarrow \{\}, d_{\text{waves}} \leftarrow \{\}, e_{\text{waves}} \leftarrow \{\}$ 
2 : Filtered = Bandpass( $PPG_{\text{signal}}$ ,  $F_1$ – $F_2$ )
3 : APG = CentralSecondDerivative(Filtered)
4 :  $APG(a_{\text{waves}}(i) - \text{cutoff} : a_{\text{waves}}(i) + \text{cutoff}) = 0$ 
5 :  $MA_{\text{peak}} = MA(APG, W_1)$ 
6 :  $MA_{\text{cde}} = MA(APG, W_2)$ 
7 : for  $n = 1$  to length( $MA_{\text{peak}}$ ) do
8 :   if  $MA_{\text{peak}}[n] > MA_{\text{cde}}[n]$  then
9 :      $BlocksOfInterest[n] = \max(APG)$ 
10 :   else
11 :      $BlocksOfInterest[n] = 0$ 
12 :   end if
13 : end for
14 : Blocks  $\leftarrow$  onset and offset from BlocksOfInterest
15 : set  $THR_1 = W_1$ 
16 : for  $j = 1$  to number of  $a_{\text{waves}} - 1$  do
17 :    $aa = a_{\text{waves}}(i + 1) - a_{\text{waves}}(i)$ 
18 :    $AC_{\text{min}} = (aa/f_s) * ac_{\text{min}}$ 
19 :    $AE_{\text{max}} = (aa/f_s) * ae_{\text{max}}$ 
20 :   SubBlocks = find( $[Blocks > b_{\text{waves}}(i) + AC_{\text{min}}] \wedge [Blocks < b_{\text{waves}}(i) + AE_{\text{max}}]$ )
21 :   Detectedwaves  $\leftarrow$  []
22 :   for  $j = 1$  to number of SubBlocks do
23 :     if width(SubBlocks[ $j$ ])  $\geq THR_1$  then
24 :       Detectedwaves = [Detectedwaves ; SubBlocks[ $j$ ]]
25 :     else
26 :       ignore SubBlocks[ $j$ ]
27 :     end if
28 :   end for
29 :   if number of Detectedwaves  $> 1$  then
30 :      $c_{\text{waves}} = \{c_{\text{waves}} ; \text{Detected}_{\text{waves}}[1]\}$ 
31 :      $e_{\text{waves}} = \{e_{\text{waves}} ; \text{Detected}_{\text{waves}}[2]\}$ 
32 :      $D \leftarrow$  minimum value between Detectedwaves[1] and Detectedwaves[2]
33 :      $d_{\text{waves}} = \{d_{\text{waves}} ; D\}$ 
34 :   else
35 :      $c_{\text{waves}} = \{c_{\text{waves}} ; \text{Detected}_{\text{waves}}[1]\}$ 
36 :      $d_{\text{waves}} = \{d_{\text{waves}} ; \text{Detected}_{\text{waves}}[1]\}$ 
37 :      $e_{\text{waves}} = \{e_{\text{waves}} ; \text{Detected}_{\text{waves}}[1]\}$ 
38 :   end if
39 : end for
40 : return ( $c_{\text{waves}}$ ,  $d_{\text{waves}}$ ,  $e_{\text{waves}}$ )

```

---

Table 2: **Pseudocode for the brute-force optimizer.** This exhaustive search systematically enumerates all possible combinations for the solution and checks whether each combination provides an optimal detector based on SE and +P.

---

**Algorithm II:** OPTIMIZER( $\text{PPG}_{\text{signal}}, f_s, a_{\text{waves}}, b_{\text{waves}}, F_1, F_2, W_1, W_2, \text{cutoff}, ac_{\text{min}}, ae_{\text{max}}$ )

---

```

1 : Initialize  $Max_{F_1} = 1, Max_{F_2} = 10, Max_{W_1} = 5, Max_{W_2} = 3 * W_1, Max_{\text{cutoff}} = 14$ 
2 : Initialize  $Max_{ac_{\text{min}}} = 8, Max_{ae_{\text{max}}} = 120$ 
3 : for  $F_1 = 0.5$  to  $Max_{F_1}$  with  $\text{step} = 0.5$  do
4 :   for  $F_2 = F_1 + 4$  to  $Max_{F_2}$  with  $\text{step} = 1$  do
5 :     for  $W_1 = 1$  to  $Max_{W_1}$  with  $\text{step} = 1$  do
6 :       for  $W_2 = 2 * W_1$  to  $Max_{W_2}$  with  $\text{step} = 1$  do
7 :         for  $\text{cutoff} = 6$  to  $Max_{\text{cutoff}}$  with  $\text{step} = 2$  do
8 :           for  $ac_{\text{min}} = 0$  to  $Max_{ac_{\text{min}}}$  with  $\text{step} = 2$  do
9 :             for  $ae_{\text{max}} = 60$  to  $Max_{ae_{\text{max}}}$  with  $\text{step} = 20$  do
10 :              DETECTOR( $\text{PPG}_{\text{signal}}, f_s, a_{\text{waves}}, b_{\text{waves}}, F_1, F_2, W_1, W_2, \text{cutoff}, ac_{\text{min}}, ae_{\text{max}}$ )
11 :              Calculate SE and +P for  $c_{\text{waves}}, d_{\text{waves}}$ , and  $e_{\text{waves}}$ 
12 :            end for
13 :          end for
14 :        end for
15 :      end for
16 :    end for
17 :  end for
18 : end for

```

---

Table 3: **A rigorous optimization over all parameters of the proposed detector: frequency band ( $F_1-F_2$ ),  $W_1$  (samples),  $W_2$  (samples), cutoff (samples),  $ac_{\min}$  (samples), and  $ae_{\max}$  (samples).** All possible combinations of parameters (26,000 iterations) have been investigated and sorted in descending order according to their overall accuracy. The data used in this training phase were PPG signals measured after 1 hour of exercise. The overall accuracy (OA) is the average value of SE and +P. Here, NaN stands for not-a-number.

Iteration	Band	$W_1$	$W_2$	Cutoff	SearchMin	SearchMax	SE	+P	OA (%)
1-60	0.5-7 Hz	1	3	6-14	2-8	80-120	98.94	100	99.47
61-135	0.5-7 Hz	2	4	6-14	0-8	80-120	98.91	100	99.46
136-150	0.5-7 Hz	1	3	6-14	0	80-120	98.82	100	99.44
151-210	1-7 Hz	1	3	12-14	2-8	80-120	98.60	100	99.30
211-225	1-7 Hz	1	3	6-14	0	80-120	98.48	100	99.24
226-300	1-7 Hz	2	4	6-14	0-8	80-120	98.36	100	99.18
301-375	0.5-7 Hz	2	6	6	0-8	80-120	98.22	100	99.11
376-450	1-7 Hz	2	6	6-14	0-8	80-120	97.67	100	98.83
.	.	.	.	.	.	.	.	.	.
.	.	.	.	.	.	.	.	.	.
.	.	.	.	.	.	.	.	.	.
.	.	.	.	.	.	.	.	.	.
25995	1-10 Hz	5	15	12	8	60	65.69	NaN	NaN
25996-25999	1-10 Hz	5	15	14	0-6	60	65.85	NaN	NaN
26000	1-10 Hz	5	15	14	8	60	65.69	NaN	NaN

Table 4: **Performance of the proposed algorithm to detect  $c$ ,  $d$ , and  $e$  waves in the testing dataset (PPG signals measured during rest).** The PPG signals were collected from 27 subjects for 20 seconds before the exercise [20]. To evaluate the performance of the proposed algorithm, two statistical measures were used:  $SE = TP/(TP + FN)$  and  $+P = TP/(TP + FP)$ , where TP is the number of true positives ( $c/d/e$  wave detected as  $c/d/e$  wave), FN is the number of false negatives ( $c/d/e$  wave has not been detected), and FP is the number of false positives (non- $c/d/e$  wave detected as  $c/d/e$  wave).

Record	$c$ waves		$d$ waves		$e$ waves	
	SE (%)	+P (%)	SE (%)	+P (%)	SE (%)	+P (%)
A1	100	100	100	100	100	100
A2	100	100	100	100	100	100
B1	100	100	100	100	100	100
B2	100	100	100	100	100	100
C2	100	100	50	100	100	100
C3	100	100	92.86	100	94.73	94.73
D2	100	100	100	100	100	100
D3	100	100	100	100	100	100
E1	100	100	100	100	100	100
E2	100	100	100	100	100	100
E3	100	100	100	100	100	100
G2	100	100	100	100	100	100
G3	100	100	100	100	100	100
H3	100	100	83.33	100	100	100
I1	100	100	100	100	100	100
I2	100	100	100	100	100	100
J2	100	100	100	100	100	100
L2	100	100	50	100	100	100
L3	100	100	100	100	100	100
N2	100	100	94.12	100	100	100
N3	100	100	85.71	100	100	100
O1	100	100	100	100	100	100
O2	93.75	93.75	60	100	93.75	93.75
P1	100	100	14.29	100	100	100
P2	100	100	100	100	100	100
Q1	100	100	100	100	100	100
Q2	100	100	100	100	100	100
27 subjects	99.82	99.82	92.71	100	99.64	99.64

## 9 Figures

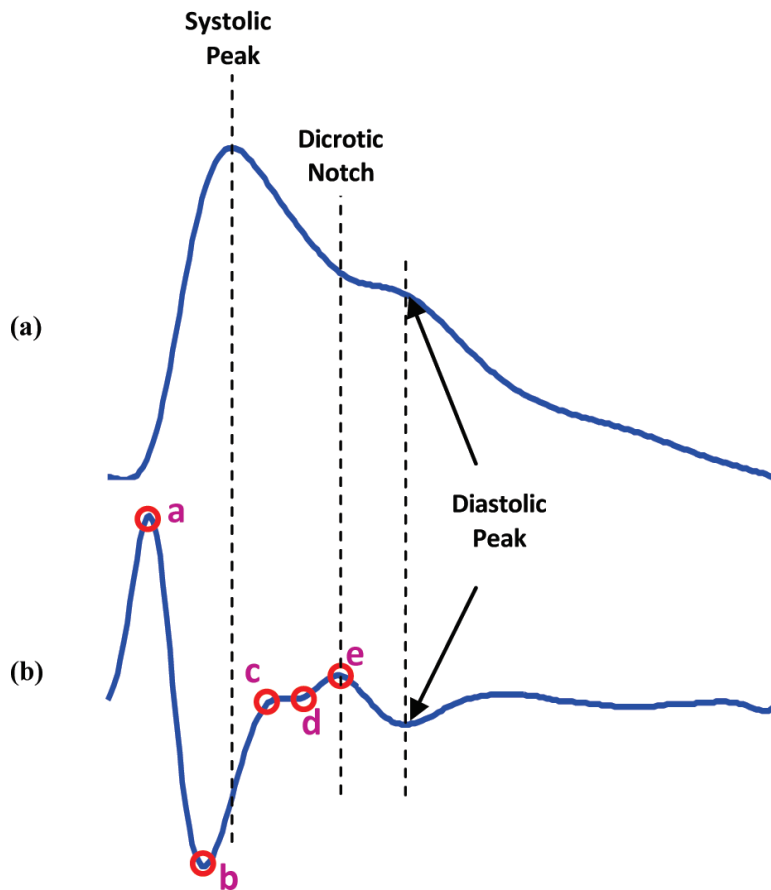


Figure 1: **Fingertip photoplethysmogram signal measurement [26].** (a) Fingertip photoplethysmogram. (b) Second derivative wave of photoplethysmogram. The photoplethysmogram waveform consists of one systolic wave and one diastolic wave, while the second derivative photoplethysmogram waveform consists of four systolic waves (*a*, *b*, *c*, and *d* waves) and one diastolic wave (*e* wave).

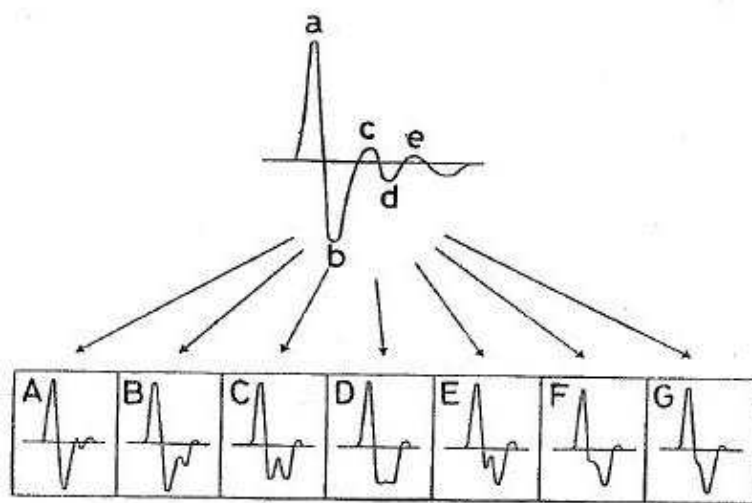


Figure 2: **APG waveforms and types of photoplethysmogram [19].** There are different types of APG waveforms. Type A (far left) refers to good circulation, whereas the amplitude of the *b* wave is lower than the *c* wave. Type B refers to good circulation but deteriorating, while type C refers to poor circulation. The last four types of APG waveforms D–G refer to distinctively bad circulation, whereas the amplitude of the *c* wave is lower than the *b* wave.

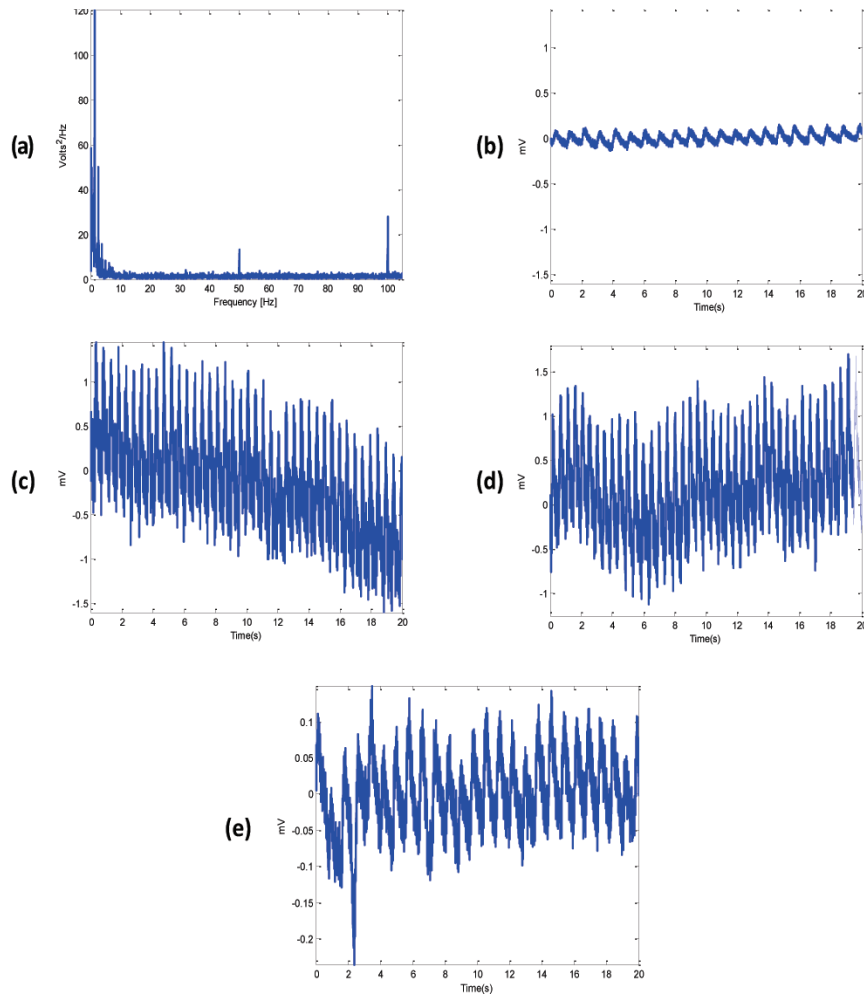


Figure 3: **Challenges in analysing PPG signals.** (a) Mains electricity noise. (b) Low amplitude PPG signals. (c) Powerline and motion artifacts in PPG signal. (d) Baseline wandering in PPG signal. (e) Premature ventricular contraction.

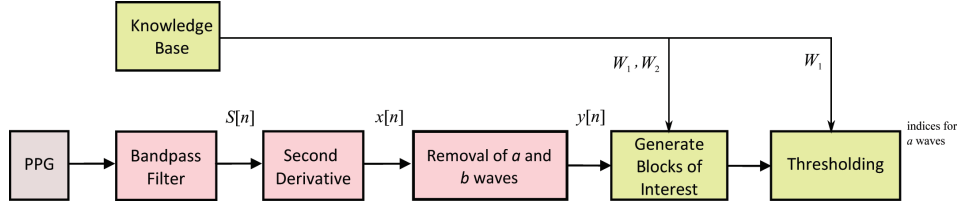


Figure 4: **Flowchart of the knowledge-based  $c$ ,  $d$ , and  $e$  waves detection algorithm.** The algorithm consists of three stages: pre-processing (bandpass filter, second derivative, and cancellation of  $a$  and  $b$  waves), feature extraction (generating blocks of interest based on prior knowledge), and thresholding (based on prior knowledge).

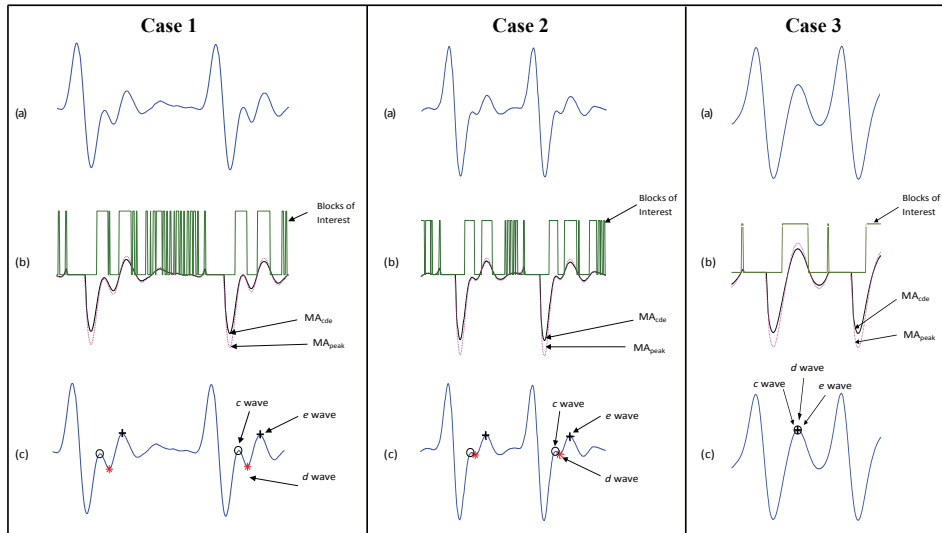


Figure 5: **Three cases of APG signals demonstrate the effectiveness of using two moving averages to detect  $c$ ,  $d$ , and  $e$  waves in different conditions.** Cases 1 and 2 occur usually in subjects measured at rest where  $c$ ,  $d$ , and  $e$  waves do exist, while case 3 usually occurs in subjects with fast heart rate where  $c$ ,  $d$ , and  $e$  waves are merged. (a) second derivative of filtered PPG signal; (b) generating blocks of interest after using two moving averages: the dotted line is the first moving average and the solid line is the second moving average; (c) the detected  $c$ ,  $d$ , and  $e$  waves after applying the thresholds.

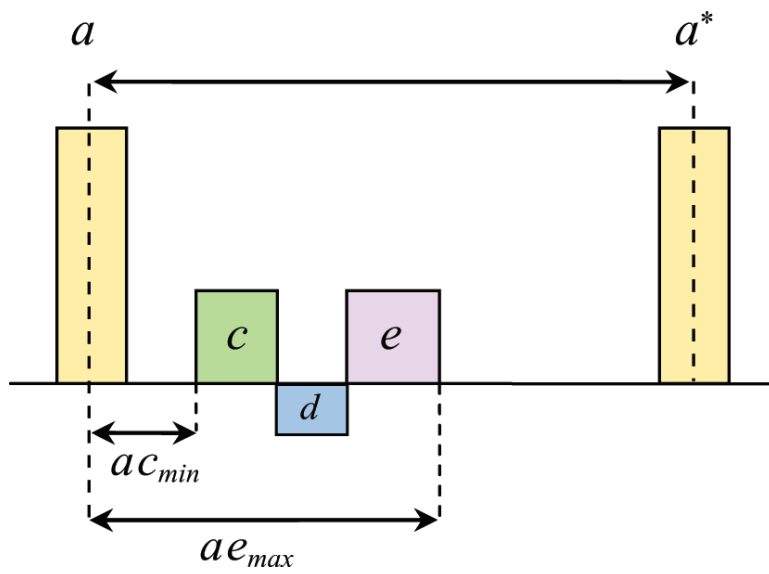


Figure 6: **Demonstrating  $c$ ,  $d$ , and  $e$  waves time occurrence regarding the current  $a$  peak and the next  $a$  peak ( $a^*$ ).** Here,  $ac_{min}$  represents the minimum interval between the current  $a$  peak and the  $c$  wave;  $ae_{max}$  represents the maximum interval between the current  $a$  peak and the  $e$  wave.

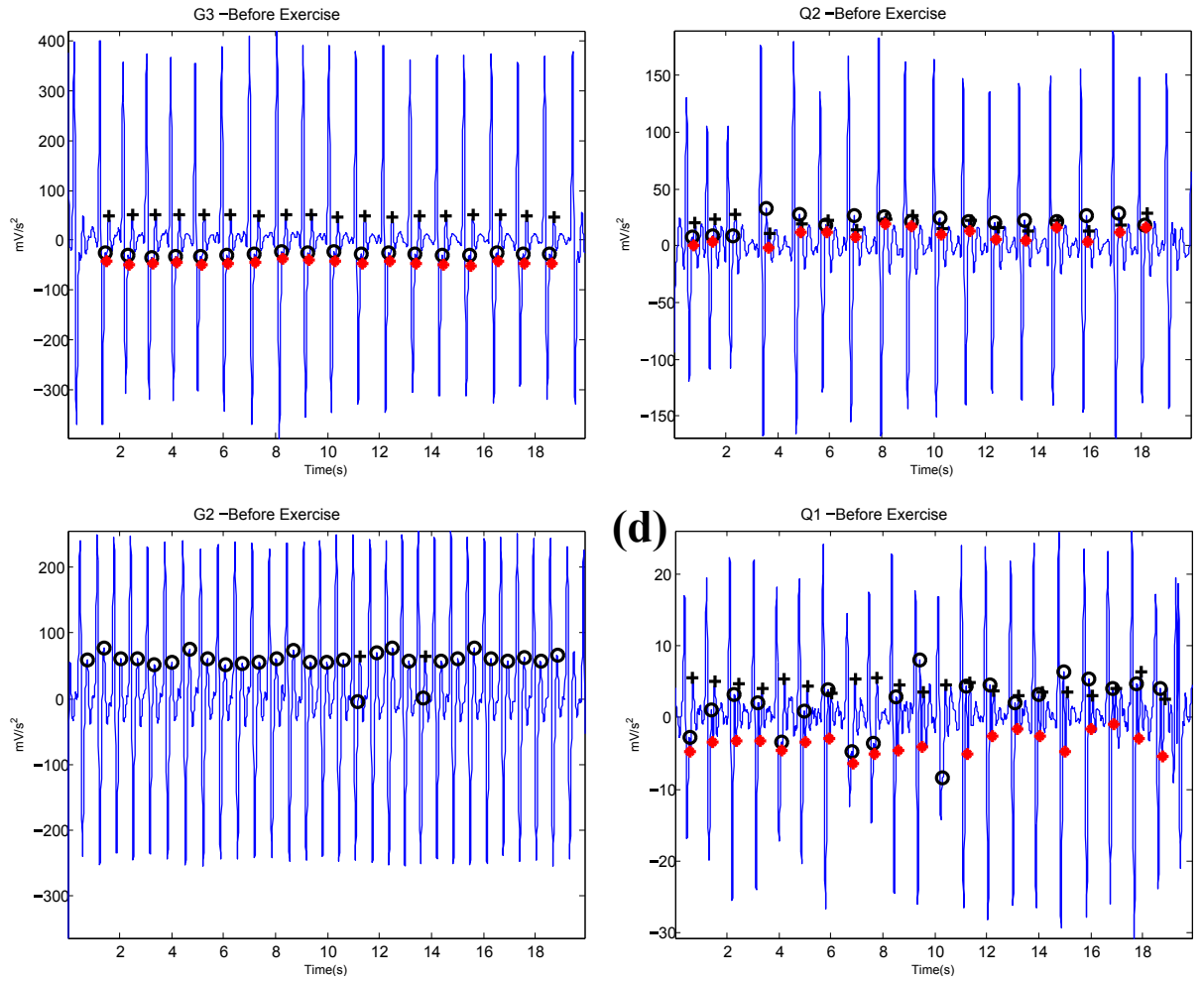


Figure 7: **Detected *c*, *d*, and *e* waves in APG signals measured during rest.** They contain (a) regular heart rhythm, (b) irregular heart rhythm, (c) fast rhythm, and (d) low amplitudes. Here, the circle represents the detected *c* wave, the '+' represents the annotated *e* wave, and the red star represents the detected *d* wave using the proposed algorithm.

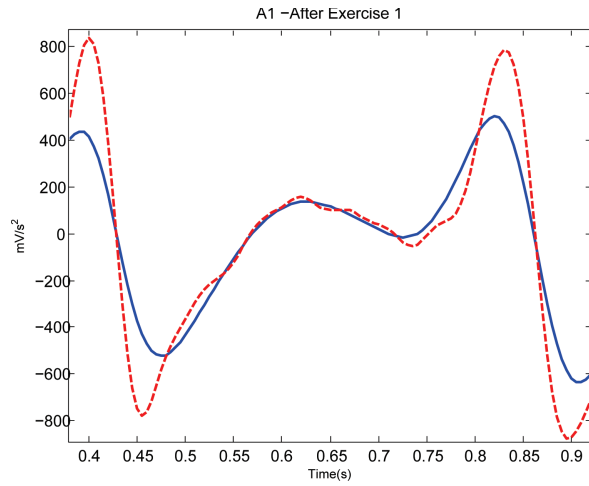


Figure 8: **One beat PPG signal measured after exercise, with fast heart rhythm (132 beats per minute), bandpass filtered at 0.5–7 Hz (solid blue line) and at 0.5–15 Hz (dashed red line).** It is clear that the merging of *c*, *d*, and *e* peaks in the case of fast heart rhythm is not caused by filtering.

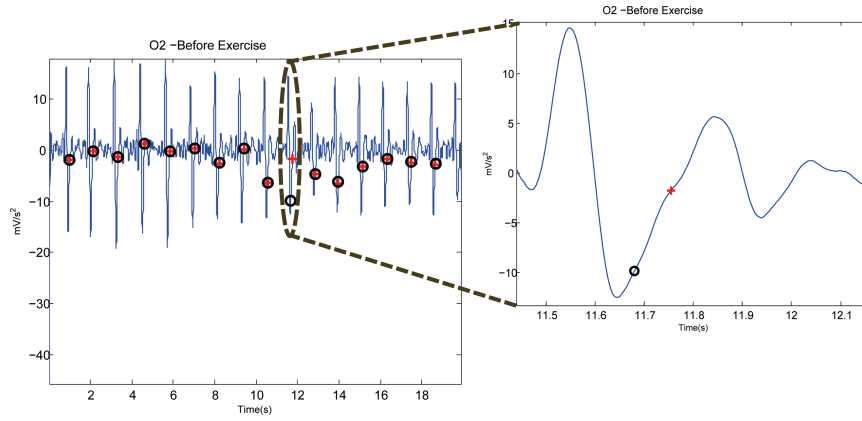


Figure 9: **Instances of failure occurring with the proposed algorithm to detect  $c$  waves in volunteer O2 during rest (before exercise).** Here, '+' represents the annotated  $c$  wave, and the circle represents the detected  $c$  wave using the proposed algorithm. If the circle is empty it means a false positive, and if the '+' does not lie in a circle it means a false negative.

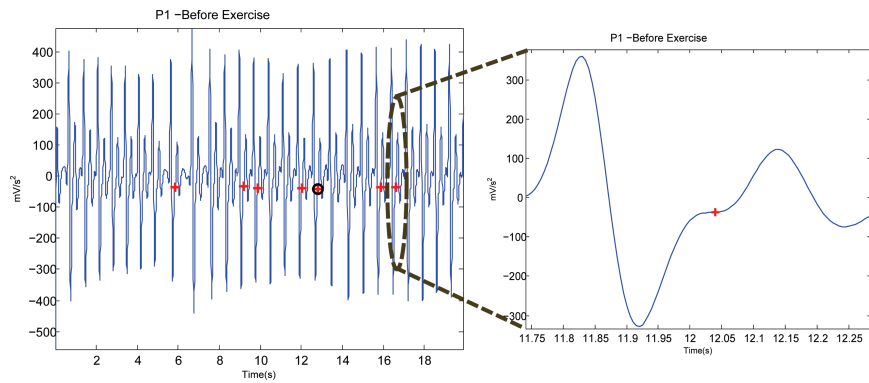


Figure 10: **Instances of failure occurring with the proposed algorithm to detect  $d$  waves in volunteer P1 during rest (before exercise).** Here, '+' represents the annotated  $d$  wave, and the circle represents the detected  $d$  wave using the proposed algorithm. If the circle is empty it means a false positive, and if the '+' does not lie in a circle it means a false negative.

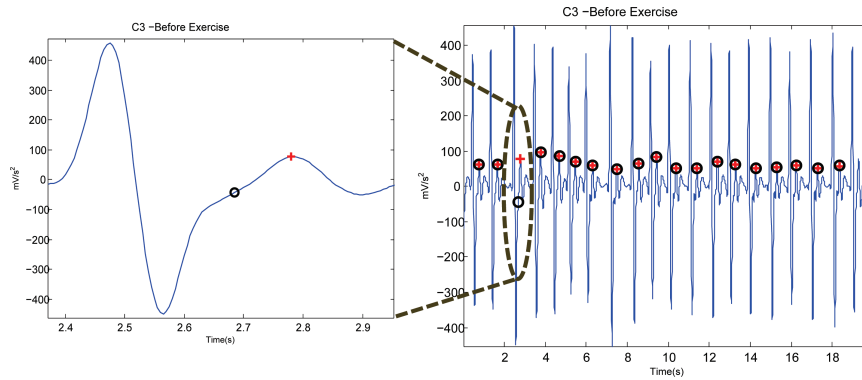


Figure 11: Instances of failure occurring with the proposed algorithm to detect  $e$  waves in volunteer C3 during rest (before exercise). Here, '+' represents the annotated  $e$  wave, and the circle represents the detected  $e$  wave using the proposed algorithm. If the circle is empty it means a false positive, and if the '+' does not lie in a circle it means a false negative.